JMB

Crystal Structure of TB-RBP, a Novel RNA-binding and Regulating Protein

John M. Pascal[1], P. John Hart[2], Norman B. Hecht[3] and Jon D. Robertus[1]*

[1]*Institute for Cellular and Molecular Biology and the Department of Chemistry and Biochemistry University of Texas at Austin Austin, TX 78712, USA*

[2]*Department of Biochemistry University of Texas Health Science Center at San Antonio San Antonio, TX 78229, USA*

[3]*Center for Research on Reproduction and Women's Health and Department of Obstetrics and Gynecology University of Pennsylvania School of Medicine Philadelphia, PA 19104, USA*

*Corresponding author

The testis/brain-RNA-binding protein (TB-RBP) spatially and temporally controls the expression of specific mRNAs in developing male germ cells and brain cells, and is implicated in DNA recombination and repair events. We report the 2.65 Å crystal structure of mouse TB-RBP. The structure is predominantly α-helical and exhibits a novel protein fold and mode of assembly. Crystal symmetry and molecular symmetry combine to form an octet of TB-RBP monomers in the shape of an elongated spherical particle with a large cavity at its center. Amino acid residues that affect RNA and DNA binding are located on the interior surface of the assembled particle, and a putative nucleotide-binding domain that controls RNA binding is located at a dimer interface. Other modes of assembly are suggested for TB-RBP based on our structure and recently reported electron microscopic reconstructions of human TB-RBP.

© 2002 Elsevier Science Ltd. All rights reserved

Keywords: X-ray structure; novel fold; RNA-binding protein; mRNA expression control

Introduction

Mammalian spermatogenesis proceeds in stages that require various forms of gene expression.[1] Early stages are frequently controlled at the level of transcription. However, transcription ceases mid-way through spermiogenesis, the haploid phase of spermatogenesis. As a result, gene expression in the later phases of male germ cell development is controlled at the level of mRNA translation. Stored mRNAs are translationally suppressed until the proteins for which they code are developmentally required. This vital process requires the action of proteins that can specifically recognize certain mRNAs and, by binding to them, prevent expression. These silencing proteins must also possess temporal and/or spatial sensors to allow appropriate release of mRNA.

Testis/brain-RNA-binding protein (TB-RBP) was identified initially as a protein able to suppress the translation of stored mRNAs that contained sequences called H and Y elements, of 14 and 15 residues, respectively, in their 3′ untranslated region or UTR.[2] The gene coding for TB-RBP has been cloned and expressed in bacteria.[3] It was found to code for a 228 residue, 26 kDa protein. In addition to exerting an influence on the temporal expression of mRNA, it was discovered that TB-RBP can influence the spatial expression of mRNA. TB-RBP can bind to and link its associated mRNAs to microtubules to facilitate movement within cells.[4] One example of this spatial control-function occurs during the haploid phases of spermatogenesis. Each spermatid has either an X or a Y chromosome that contains essential genes. Therefore, there is a need to share genetic information between haploid spermatids. TB-RBP has been shown to cross through intercellular bridges between developing haploid spermatids and is thus thought to be involved in maintaining genetic equivalence between spermatids.[5] TB-RBP appears to act as an adaptor molecule in tubulin-mediated transport of mRNA. It is abundant in brain cells,

where it binds to the 3′ UTR of translationally suppressed and transported brain mRNAs.[6]

Translin is the human orthologue of TB-RBP; they are nearly 99% identical in sequence, differing at just three amino acid positions. Translin binds single-stranded DNA (ssDNA) sequences found near breakpoint regions in recombination hot spots.[3,7] Such binding has been implicated in gene translocation events in myeloid leukemia cell lines, where high levels of TB-RBP are found in the nucleus.[7] The exact nature of the ssDNA binding by TB-RBP/translin is not known but the localization of TB-RBP/translin to the nucleus in pachytene spermatocytes implicates its function in meiotic DNA recombination and repair events.[8] The ability of TB-RBP, and translin, to bind to mRNA and DNA is mediated by a conserved basic sequence RFHEH, which lies between residues 86 and 90.[9,10]

In accomplishing its varied functions, TB-RBP interacts with mRNA and with a variety of signal molecules and proteins. It now appears that TB-RBP binding of mRNA may be regulated by GTP. It has been shown that a TB-RBP·GDP complex will bind RNA, but binding of GTP releases it. Mutagenic alteration of the guanine nucleotide site prevents RNA binding, presumably because it prevents GDP binding.[11] TB-RBP/translin is known to interact with TRAX, a structural homologue that does not bind mRNA.[12] Formation of hetero-oligomers between TB-RBP and TRAX releases bound mRNA.[10] Immunoprecipitation with anti-TB-RBP antibodies precipitated complexes with cytoskeletal γ-actin.[13] This is consistent with the notion that TB-RBP serves as an adaptor during transport of mRNA through cytosolic bridges between developing male germ cells. Very recently, the Hecht group used immunoprecipitation to demonstrate that TB-RBP associates with a microtubular motor protein that is a KIF isoform (unpublished results). KIF proteins are members of the kinesin family,[14] and this observation suggests strongly that TB-RBP can act as an adapter to link specific mRNAs to a neuronal motor transport system. To date, no high-resolution structure of TB-RBP, translin, or any related protein has been solved. Here, we present the 2.65 Å crystal structure of TB-RBP and describe its novel fold and mode of assembly.

Results and Discussion

TB-RBP structure determination

Multi-wavelength anomalous diffraction (MAD) data from a methyl mercury derivative crystal provided experimental phases for TB-RBP structure determination (Table 1). There are four TB-RBP monomers in an asymmetric unit, and this 4-fold molecular symmetry was used to modify and improve experimental phases. Electron density maps produced with the modified experimental

phases were of high quality and allowed a majority of the atomic model to be constructed (Figure 1(a)). The final model consists of 854 amino acid residues from four TB-RBP monomers, and 82 solvent molecules. The model refined to an R_{work} and R_{free} of 24.7% and 29.0%, respectively (Table 1).

TB-RBP has a highly helical secondary structure; there are seven helices that constitute >70% of the protein's amino acid residues (Figure 1(b) and (c)). Helix 3 acts as the central core of the molecule. Helices 1 and 2 are anti-parallel to each other, and lie on one side of helix 3. On another side of helix 3 is a three-helix bundle (helices 5, 6, and 7) that forms the C terminus of the protein. Helix 4 is between two short random coil areas that rest along a side of helix 3. Between helix 2 and helix 3 is an extended region of random coil that is involved in a dimer interface. The length of the molecule is roughly 80 Å, while the globular portion is approximately 20 Å × 35 Å × 50 Å. The four monomers of the asymmetric unit have very similar folds. The r.m.s. deviations for superimposing C^{α} positions for monomers B, C, and D onto monomer A are 0.37 Å, 0.56 Å, and 0.41 Å, respectively.

TB-RBP intermolecular interactions

The C terminus of TB-RBP has been shown to be involved in dimerization.[9,15] The spacing of five leucine residues and a valine residue in the C terminus led to speculation that it was a leucine zipper domain (Figure 1(c)). Most of these residues, in the apoTB-RBP structure, are involved in intramonomer contacts in the three-helix bundle of the C terminus, ruling out the leucine zipper in dimerization. However, the C termini of TB-RBP monomers do interact in the crystal structure in another way. The C termini of the four monomers of the asymmetric unit associate around a pseudo 4-fold axis, with each of the C termini interacting in a similar manner (Figure 2(a) and (b)). The C-terminal residues Val156, Val159, Thr160, Leu184, Leu212, and Ile214 of the three-helix bundle, along with residues Gln29, Arg36, and Gln43 from helix 1, contribute to interactions involving the C termini. Point mutations changing either Leu184 (helix 6) or Leu191 (helix 7) to proline results in loss of multimeric structure and loss of DNA binding in human translin.[9] Presumably, altering these residues disrupts the helices in a way that perturbs the C-terminal dimer interactions. Taken together, C-terminal interactions bury 730 Å² of accessible surface area per monomer.

Approximately ten residues (~219–228) of the C terminus of each TB-RBP monomer are not ordered in the crystal structure and extend into a solvent region. It may be that the crystallization conditions do not favor a stable conformation for these residues, or they may only be well-ordered when DNA or RNA is present. *In vitro* experiments suggest TB-RBP dimers can be linked by a disulfide

Table 1. Summary of crystallographic data

				MeHg derivative		
Data collection	High res. native	Low res. native	Xenon derivative	Peak	Inflection	Remote
Resolution (Å)	2.65	3.15	3.6	3.0	3.0	3.0
Wavelength (Å)	0.9794	1.5418	1.5418	1.0052	1.0094	0.9892
Observations	193,026	94,630	98,698	179,837	149,010	231,835
Unique observations	34,219	21,349	27,145[a]	46,162[a]	45,908[a]	46,219[a]
Completeness (%)[b]	95.3 (98.1)	99.3 (99.1)	99.4 (96.3)	98.4 (96.8)	98.1 (95.7)	99.5 (98.3)
Average I/σ_b	29.7 (2.9)	26.7 (2.7)	15.0 (2.4)	17.3 (3.1)	14.3 (2.9)	19.6 (3.2)
R_{merge}[b,c]	4.5 (45.7)	5.3 (45.8)	7.9 (43.8)	6.4 (35.4)	7.1 (37.5)	6.7 (40.7)
Figure of merit[d]				0.55		

Refinement	
Resolution (Å)	20.0−2.65
R_{work}[e]	0.247 (33,232)
R_{free}[e]	0.29 (1741)
Number of protein residues/atoms	854/7013
Number of ordered waters	82

r.m.s deviations from ideal[f]	
Bonds (Å)	0.0072
Angles (deg.)	1.08

Ramachandran plot[g]	
Most favored (residues)	720
Allowed (residues)	66
Disallowed (residues)[h]	1

Modeled residues

Monomer	Residues modeled	Residues modeled as Ala	Average B factor (Å²)
A	1−46 and 53−218	Arg129, Lys131, Lys193, Lys199, Asp218	67.1
B[h]	−3 to −1 and 1−218	Lys131, Asp218	67.2
C	1−45 and 53−217	Lys56, Glu63, Arg129, Glu130	93.8
D	1−47 and 53−216	Lys26, Arg129, Lys131, Lys187	96.5

[a] Bijvoet pairs listed separately.
[b] Values in parentheses are for the highest-resolution shell.
[c] $R_{\mathrm{merge}} = \sum_{hkl}\sum_i |I_i(hkl) - \langle I(hkl)\rangle| / \sum_{hkl}\sum_i I_i(hkl)$.
[d] Reported by SOLVE.[20]
[e] R_{work} and $R_{\mathrm{free}} = \sum_{hkl}|F_{\mathrm{obs}} - F_{\mathrm{calc}}| / \sum_{hkl}|F_{\mathrm{obs}}|$; calculated with number of reflections shown in parentheses.
[f] Determined using CNS.[24]
[g] gDetermined using PROCHECK.[25]
[h] The N terminus has seven extraneous residues from cloning. In monomer B, three of these residues are ordered (labeled −3 to −1). Residue B −2 is forced by a symmetry contact into an unfavorable conformation.

between two Cys225 residues in this segment.[15] Dissolved TB-RBP crystals migrate as a dimer on non-reducing polyacrylamide gels (data not shown), suggesting the C terminus is still intact and bonded in the crystal. However, it is not clear that a disulfide bond could form in the reducing environment of the cytoplasm, and this Cys is not conserved in TB-RBP homologues from other species.

GTP control of molecular assembly

In the presence of GTP or GTPγS, TB-RBP binding to RNA is reduced 50% (GTP) and 90% (GTPγS) compared to TB-RBP alone or with GDP present.[11] A putative GTP-binding domain has been located between residues 159 and 163 (VTAGQ) based on similarity to the GTP-binding motif of Ras proteins.[11] TB-RBP will no longer bind GTP when this sequence is mutated to VTNSD.[11] Our crystals crack and disintegrate when soaked in the presence of GTP or GTPγS, most likely indicating a large change in molecular arrangement. Residues 159 to 163 lie between helices 5 and 6, an area that is involved in the C-terminal interactions (Figures 1(b) and 2(b)). GTP binding to this region of the molecule could disrupt this interaction and thus control molecular assembly. The putative GTP-binding sequence is
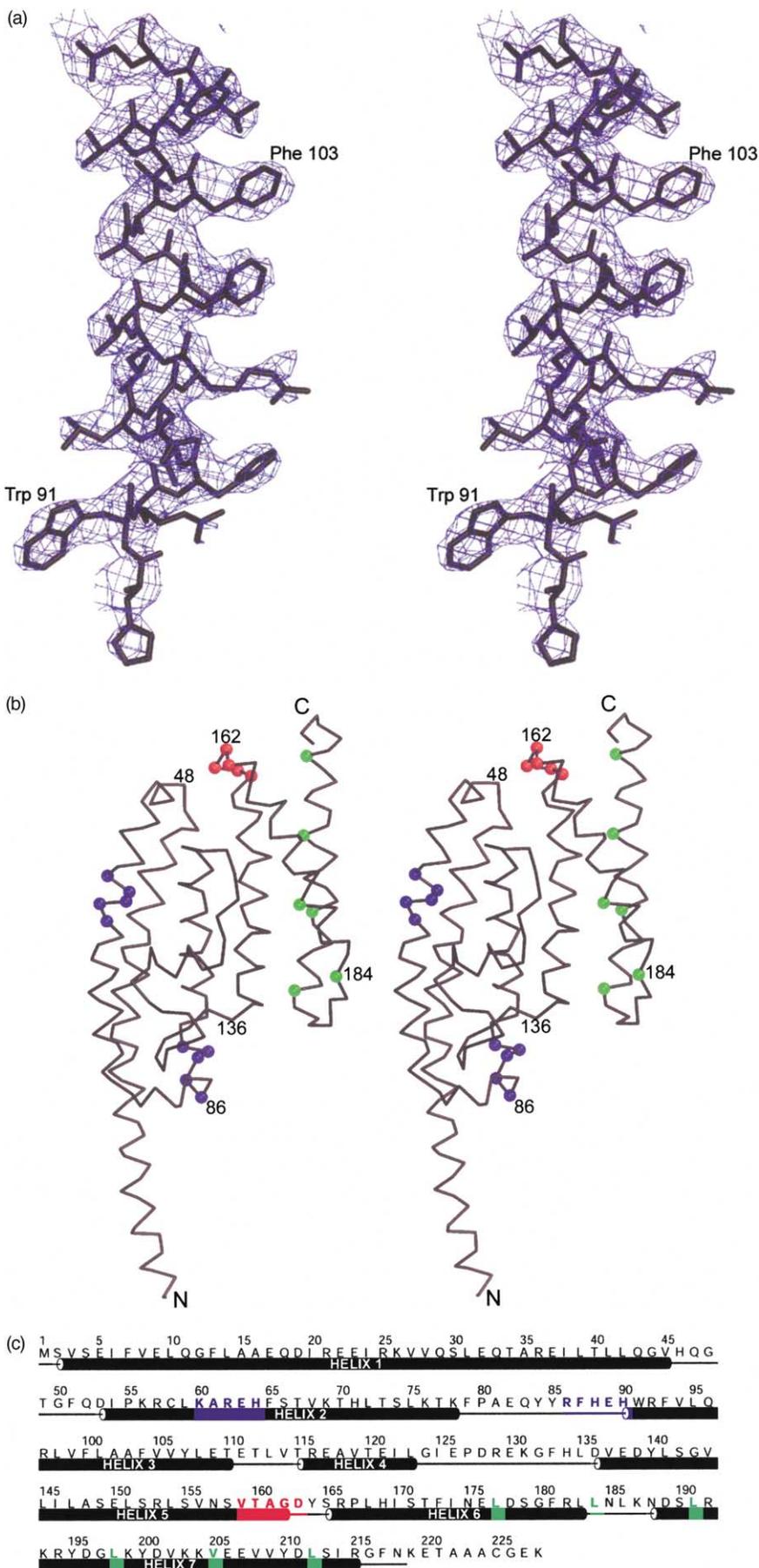
Figure 1. Structure of a TB-RBP monomer. (a) A stereoview of electron density for residues 90–109 of α-helix 3. The map was constructed with native amplitudes and dm-modified[21] experimental phases from the MeHg MAD data. The map is contoured at 1.2σ, and the final model is overlaid in thick bonds. (b) A Cα trace for residues 1–218 of monomer B of the TB-RBP structure, viewed in stereo. The termini are labeled and several Cα positions are numbered. Cα positions of several notable residues are distinguished by colored spheres: blue spheres indicate residues proposed to interact with nucleic acid; red spheres indicate residues of the putative nucleotide-binding domain; and green spheres indicate residues of the hypothetical leucine zipper domain. (c) A schematic representation of TB-RBP secondary structure. Greater than 70% of the protein's residues are in α-helical conformations. The seven helices are labeled and are represented by cylinders. Random coil regions are represented by lines. Residues 219–228 were not visible in electron density maps. The colored residues follow the convention in (b). This picture was made using ALSCRIPT.[30]
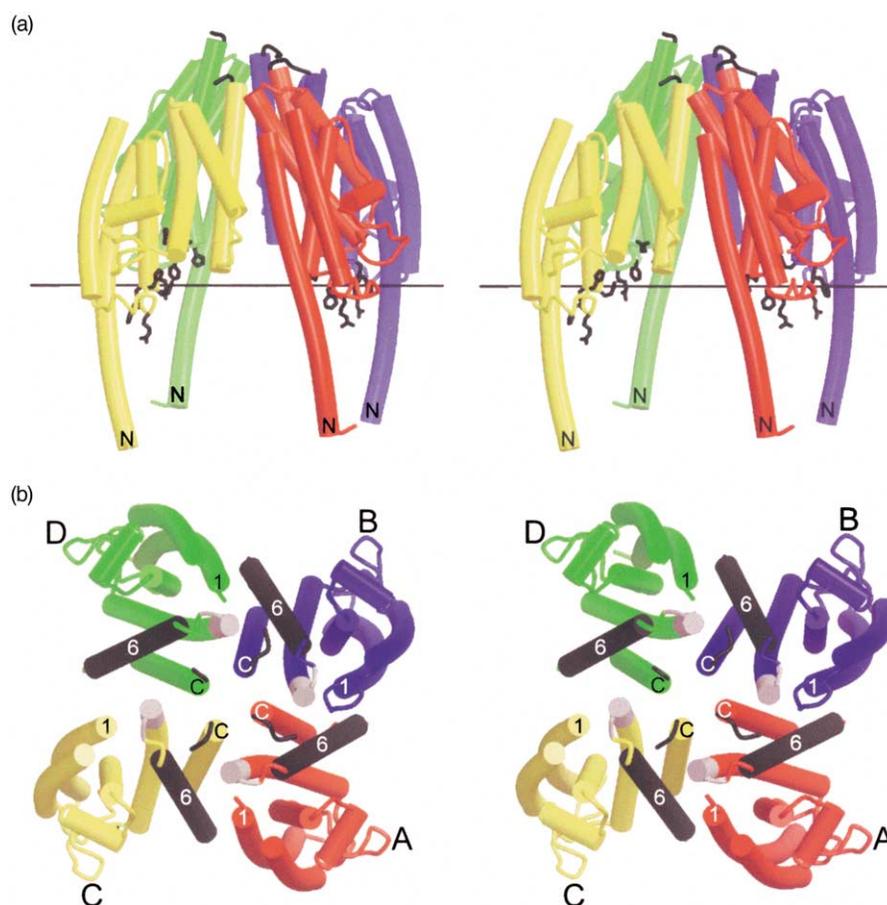
Figure 2. The TB-RBP asymmetric unit: C-terminal interactions. (a) Monomers A, B, C, and D are colored red, blue, yellow, and green, respectively. The N termini are labeled and the C termini are colored black. The C termini of the monomers interact around a pseudo 4-fold axis, located approximately vertically in the plane of the page. Each of the N termini extends in the same direction. Residues known to affect both ssDNA and RNA binding are drawn in black bonds and face the interior of the ring. This assembly could roughly approximate the assembly seen in electron microscopy reconstructions.[16] There would need to be some alteration in order to open the ring to allow eight monomers. The solid line represents the 2-fold crystallographic axis. Rotation about this axis creates a prolate, ellipsoidal particle, consisting of eight TB-RBP monomers. That particle is roughly 10.5 nm along its longest axis and 8 nm along its shortest axis. A large cavity is formed at the center of the particle. (b) The same tetramer as in (a), rotated 90° toward the viewer around a horizontal axis in the plane of the page. The region of the putative guanine nucleotide-binding domain is colored grey in each of the monomers to show its involvement in C-terminal interactions. The N terminus of helix 1 of each monomer is labeled, and helix 6 is colored black and labeled. Helix 1 of monomer C has little contact with helix 6 of monomer D. The other C-terminal interactions around the pseudo 4-fold involve these same helices more extensively. This discrepancy highlights the deviation in interaction surface area between monomers C and D (370 $\mathring{A}^2$) as compared to the interaction surface areas between monomers A and C (730 $\mathring{A}^2$), monomers A and B (770 $\mathring{A}^2$), and monomers B and D (690 $\mathring{A}^2$). This may indicate that a ring of four monomers can open to form a larger ring of monomers, as seen in electron microscopy images.[16]

invariant in the four known TB-RBP/translin sequences.

Comparison with electron microscopy studies

Recent electron microscopy studies with human TB-RBP (translin) have shown that translin forms a C8 ring of eight monomers in the absence or presence of ssDNA or RNA.[16] One face of the translin ring has a large opening (~ 50 Å), and the other has a smaller opening (~ 30 Å). A 24 base ssDNA oligomer or a 39 base RNA fragment, containing Y and H elements, were seen to fill the central cavity of the translin octamer. The asymmetric unit of our structure, containing roughly 4-fold cyclic C-terminal interactions (Figure 2(a)), may resemble some interactions of the monomers seen in the electron micrograph reconstructions. The globular portions of TB-RBP monomers would form the bulkier end of the ring with the small opening, while the N termini interacting to form the smaller end of the ring with the larger opening (Figure 2(a)). Forming an 8-fold ring would require an "opening" of our ring of four monomers. In our pseudo 4-fold structure, interface CD buries only 370 $\mathring{A}^2$, compared to nearly 750 $\mathring{A}^2$ for the other interactions (Figure 2(b)). This suggests that the 4-fold ring we observe is under strain and could
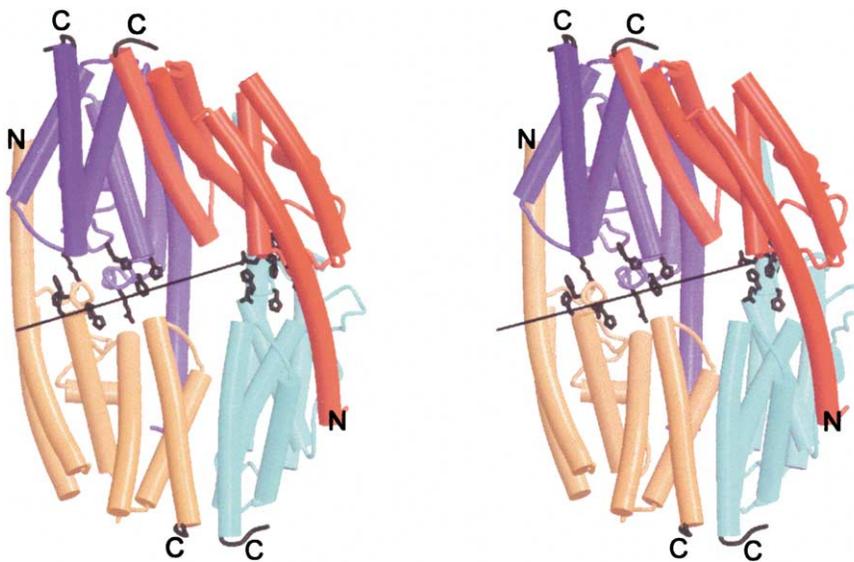
Figure 3. Molecular interactions of the TB-RBP structure. Monomers A (red) and B (blue) generate symmetry-related monomers A′ (orange) and B′ (cyan) by rotation about the crystallographic 2-fold axis (the same as shown in Figure 2(a) is drawn here). The N terminus of helix 1 of monomer A interacts with B′, near its three-helix bundle. Monomer B′ makes the same interactions with A. This dimerization of TB-RBP buries over 1700 $Å^2$ of accessible surface area per monomer. Monomers C and D dimerize similarly. Dimer AB′ and dimer A′B make C-terminal interactions to form a tetramer with a continuous surface, shaped like a cupped hand. Residues known to affect both ssDNA and RNA binding (drawn in black bonds) form a "belt" on the concave surface of the tetramer. The concave surfaces of two such tetramers come together (two cupped hands) to form the large cavity at the center of the ellipsoidal TB-RBP octamer.

"open" to form a larger ring containing additional monomers. A fitting of the TB-RBP model with electron microscope data is being undertaken and will be described in detail elsewhere.

Two basic regions of TB-RBP have been implicated in nucleic acid interaction: residues 86–92 (RFHEHWR) and residues 60–64 (KAREH).[9,10] Modifying the former segment disrupts RNA and DNA complex formation, but still allows TB-RBP aggregation.[9,1] These residues are on the N-terminal end of helix 3, positioned towards the center of the TB-RBP tetramer ring, where they might interact with nucleic acid enclosed within the ring (Figure 2(a)); they are invariant in the four known TB-RBP/translin sequences. The basic residues from 60 to 64 were proposed to affect RNA-binding.[10] They are located on helix 2 (Figure 1(b) and(c)) and face the outside of the ring of four monomers. These residues are unlikely to interact with the specific nucleic acid residues of the Y and H elements that TB-RBP recognizes. However, they may play a role in non-specifically organizing extended segments of bound mRNA.

An octamer of TB-RBP monomers in the crystal

In addition to the pseudo 4-fold aggregation, a second kind of TB-RBP interaction is seen in our crystals. The N terminus of helix 1, a region of the C-terminal three-helix bundle, and the extended random coil region between helix 2 and helix 3 are involved in an extensive crystallographic 2-fold dimerization interface. This interaction is shown in Figure 3. For clarity, only the A and B monomers from Figure 2(a) are shown in red and blue in Figure 3. The crystallographic 2-fold generates A′ and B′ as orange and cyan units. Helix 1 of monomer A interacts between helix 5 and helix 6

of monomer B′, and monomer B makes the same, largely hydrophobic, contacts with A′. Residues 82 to 86 from each monomer form another region of close interaction. The main-chain atoms of residues Tyr85 and Arg86 are in close contact, and the aliphatic portion of the Arg side-chain interacts with the Tyr side-chain. There are several electrostatic interactions involved in the dimer interface. The entire contact surface buries roughly 1700 $Å^2$ of accessible surface area per monomer. It should be noted that these four units create a concave surface, like a cupped hand. In fact, all four monomers of the AU (Figure 2(a)) interact *via* the crystallographic operator to form a closed octamer (two cupped hands). That is, four crystallographic dimers rotate around a pseudo 4-fold axis, juxtaposing their C termini in similar manners. The resulting octamer creates a prolate ellipsoid particle roughly 10.5 nm along its long axis, and 8.0 nm along its short axis. The concave surfaces of two tetramers create a cavity roughly 20 Å across at the center of the particle. Interestingly, basic residues 86 to 90, known to affect TB-RBP·RNA and TB-RBP·DNA complex formation, face the interior of the central cavity formed by the crystalline TB-RBP octamer (Figure 3). The basic residues from each monomer in an octamer form a "belt" around the interior surface; this is illustrated in Figure 4. The interior cavity of the crystalline octamer can easily contain an 18 base RNA structure, the size of the Y and H elements recognized by TB-RBP. However, it is not clear that a more extended RNA could enter or exit the prolate ellipsoid form of TB-RBP. The crystalline form lacks a channel that could accommodate even a single strand of nucleic acid.

TB-RBP functions as an octamer, as shown by size-exclusion column studies,[9] electron microscopy,[16] and analytical ultracentrifugation.[17]
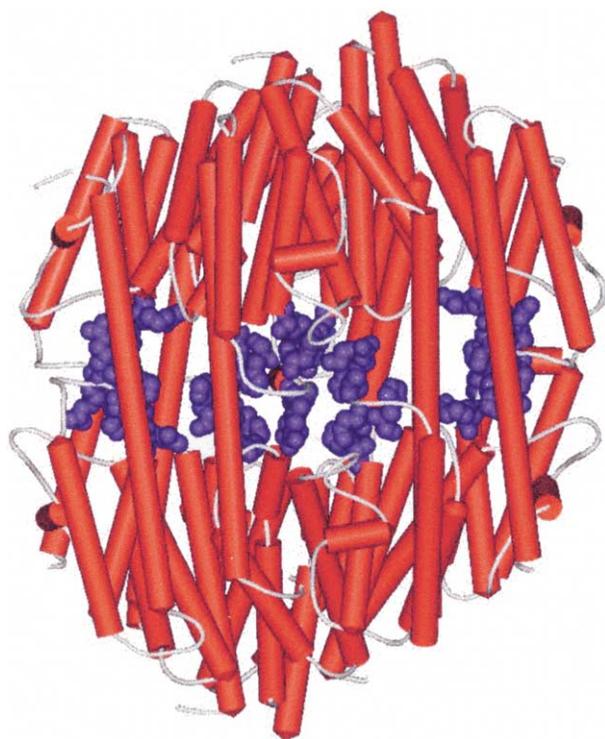
Figure 4. The position of the putative RNA-binding residues in the TB-RBP octamer. The protein backbone is displayed as a cartoon, with the α-helices shown as thin cylinders. The positively charged residues of the putative RNA-binding segment are emphasized as blue space-filling groups.

Recent work determined the stoichiometry of TB-RBP binding DNA to be 8:1.[17] The C8 assembly seen in electron micrographs[16] was shown to contain nucleic acid within its ring structure. It is likely that this ring is the biologically relevant organization, and that our crystal structure approximates this C8 assembly with its 4-fold cyclic ring of monomers. However, the ellipsoidal octamer in our crystal seems so stable that it may have significance. It may serve as a storage form for the protein, or serve as an intermediate in the assembly of TB-RBP·RNA complexes. It may be that the GTP/GDP-induced conformational changes described above play a yet to be determined role in such an assembly. The crystalline octamer provides a cavity large enough to accommodate the Y and H elements, and places known nucleic-acid interacting residues adjacent to the potential binding cavity. Crystal complexes of TB-RBP·RNA and TB-RBP·DNA will help define the octamer assembly that specifically recognizes nucleic acids.

RNA-binding proteins are not well-represented in the protein structure database, although their function in cell development and control of gene expression is becoming increasingly apparent. The crystal structure of TB-RBP has revealed a novel protein fold within this class of proteins. The structure has given insights into the nature of the

assembly of TB-RBP. Despite its small size, the ability of TB-RBP to form large assemblies may allow it to sequester mRNA and prevent translation. The large surface of its assembly might also allow specific interactions with a variety of other proteins known to modulate its activity and help perform its function of mRNA localization.

Materials and Methods

Crystal preparation and data collection

TB-RBP was purified and crystallized as described.[18] The crystals belong to orthorhombic space group $P2_12_12$ with the following cell constants: $a = 97.2$ Å, $b = 135.5$ Å, $c = 92.2$ Å. Prior to collecting diffraction data, crystals were transferred from artificial mother liquor (0.8 M NH_4SO_4, 100 mM sodium acetate, pH 4.6) to cryo-solution (10% (w/v) PEG 4000, 30% (v/v) glycerol, 100 mM sodium acetate, pH 4.6), and then flash-cooled in liquid N_2. A methyl mercury derivative was prepared by including 0.2 mM methyl mercury acetate in the cryo-solution and leaving the crystal in the cryo-solution for 12 hours. A xenon derivative was prepared by incubating a crystal in cryo-solution in a Xenon Chamber (Hampton Research) charged to 350 psi (1 psi ≈ 6.9 kPa) for 45 minutes. Xe derivative data and low-resolution native data were collected on a Rigaku Raxis IV image plate detector with a Rigaku RU200 rotating copper anode generator (Molecular Structure Corporation, Woodlands, TX) operated at 50 kV and 100 mA. The high-resolution native data were collected on an ADSC Quantum 4 CCD detector at the X12B beamline of the National Synchrotron Light Source (NSLS), Brookhaven National Laboratory.[18] A three-wavelength MAD (multi-wavelength with anomalous dispersion) experiment was conducted with the MeHg derivative at NSLS beamline X8C. All data were processed using DENZO/SCALEPACK.[19] Table 1 summarizes the diffraction data statistics.

Structure determination, model building and refinement

Four mercury sites were found by an automated Patterson search in SOLVE[20] using MAD data between 20 and 4.5 Å. The CCP4 suite of programs[21] was used to refine the Hg atomic positions and calculate MAD phases using MLPHARE, and to perform non-crystallographic symmetry (NCS) averaging, solvent flattening, histogram mapping, and multi-resolution modification using dm. A mask approximating one monomer was created using MAMA.[22] A rough estimate for NCS operators was determined by inspection of the bones tracing, the Hg sites, and a self-rotation function from MOLREP.[21] The NCS operators were refined using IMP.[22] Using SCALEPACK,[19] the high-resolution native data were combined with low-resolution native data that had more complete and well-measured low-order reflections. The R_{merge} was 13.6%. Combining the two native data sets was essential for dm[21] to substantially improve phases. These improved phases produced an interpretable map with clear helical and side-chain density. Using O,[23] 208 residues were built into the electron density of one monomer, using all four copies of TB-RBP for verification and interpretation of poorly defined areas. This monomer was refined in CNS[24]

using a maximum likelihood target, conjugate gradient minimization, torsion angle-restrained molecular dynamics, a bulk solvent correction, and a strict NCS definition. CNS[24] σA-weighted maps, and maps produced from MAD phases combined with calculated phases in SIGMAA,[21] were used to build additional portions of the model. As a means of verifying the interpretation of the electron density maps, eight Xe sites were found by difference Fourier analysis using MeHg-MAD phases. The Xe sites were located in hydrophobic areas of the model and obeyed the NCS operators. Strict NCS was replaced with NCS restraints during refinement in order to account for regions of the monomers that did not strictly obey the molecular symmetry. Each monomer was manually adjusted in O,[23] and the force constant on NCS restraints in CNS[24] was slowly lowered as warranted by a lowering of the R_{free}. Two loop regions were difficult to model: residues 45–53 and residues 126–132. Some of these residues were modeled as alanine due to a lack of side-chain density, and some were not modeled due to a lack of main-chain or side-chain electron density. The N terminus has six extraneous residues from cloning. In monomer B, three of these residues were well-ordered and were modeled as residues -3 to -1. The C-terminal ten or so residues of each monomer were not visible. The average temperature factor for all protein atoms was 81 Å^2. This is consistent with the Wilson plot for the data and an estimate from dm[21] based on electron density variation at several levels of resolution. The electron density for monomers C and D was of lesser quality than the electron density for monomers A and B. Monomers C and D correspondingly had higher average temperature factors (Table 1). The geometry and stereochemistry of the models were analyzed throughout model building and refinement with the programs PROCHECK[25] and ERRAT.[26] The model and refinement statistics are shown in Table 1. All pictures and drawings were constructed using MOLSCRIPT[27], BOBSCRIPT,[28] and Raster3D.[29]

Protein Data Bank, accession code

The atomic coordinates for TB-RBP have been deposited in the RCSB Protein Data Bank, with accession code 1key.

Acknowledgments

References

1. Hecht, N. B. (1998). Molecular mechanisms of male germ cell differentiation. *BioEssays*, **20**, 555–561.
2. Kwon, Y. K. & Hecht, N. B. (1991). Cytoplasmic protein binding to highly conserved sequences in the 3′ untranslated region of mouse protamine 2 mRNA, a translationally regulated transcript of male germ cells. *Proc. Natl Acad. Sci. USA*, **88**, 3584–3588.
3. Wu, X. Q., Gu, W., Meng, X. & Hecht, N. B. (1997). The RNA-binding protein, TB-RBP, is the mouse homologue of translin, a recombination protein associated with chromosomal translocations. *Proc. Natl Acad. Sci. USA*, **94**, 5640–5645.
4. Han, J. R., Yiu, G. K. & Hecht, N. B. (1995). Testis/brain RNA-binding protein attaches translationally repressed and transported mRNAs to microtubules. *Proc. Natl Acad. Sci. USA*, **92**, 9550–9554.
5. Morales, C. R., Wu, X. Q. & Hecht, N. B. (1998). The DNA/RNA-binding protein, TB-RBP, moves from the nucleus to the cytoplasm and through intercellular bridges in male germ cells. *Dev. Biol.* **201**, 113–123.
6. Han, J. R., Gu, W. & Hecht, N. B. (1995). Testis-brain RNA-binding protein, a testicular translational regulatory RNA-binding protein, is present in the brain and binds to the 3′ untranslated regions of transported brain mRNAs. *Biol. Reprod.* **53**, 707–717.
7. Aoki, K., Suzuki, K., Sugano, T., Tasaka, T., Nakahara, K., Kuge, O. *et al.* (1995). A novel gene, Translin, encodes a recombination hotspot binding protein associated with chromosomal translocations. *Nature Genet.* **10**, 167–174.
8. Hecht, N. B. (2000). Intracellular and intercellular transport of many germ cell mRNAs is mediated by the DNA- and RNA-binding protein, testis-brain-RNA-binding protein (TB-RBP). *Mol. Reprod. Dev.* **56**, 252–253.
9. Aoki, K., Suzuki, K., Ishida, R. & Kasai, M. (1999). The DNA binding activity of translin is mediated by a basic region in the ring-shaped structure conserved in evolution. *FEBS Letters*, **443**, 363–366.
10. Chennathukuzhi, V. M., Kurihara, Y., Bray, J. D. & Hecht, N. B. (2001). Trax (Translin associated factor X), a Primarily Cytoplasmic Protein, Inhibits the Binding of TB-RBP (Translin) to RNA. *J. Biol. Chem.* **276**, 13256–13263.
11. Chennathukuzhi, V. M., Kurihara, Y., Bray, J. D. & Hecht, N. B. (2001). Altering the GTP binding domain of the DNA/RNA-binding protein, translin/TB-RBP, decreases RNA binding and may create a dominant negative phenotype. *Nucl. Acids Res.* **29**, 4433–4440.
12. Aoki, K., Ishida, R. & Kasai, M. (1997). Isolation and characterization of a cDNA encoding a translin-like protein, TRAX. *FEBS Letters*, **401**, 109–112.
13. Wu, X. Q., Lefrancois, S., Morales, C. R. & Hecht, N. B. (1999). Protein–protein interactions between the testis brain RNA-binding protein and the transitional endoplasmic reticulum ATPase, a cytoskeletal gamma actin and Trax in male germ cells and the brain. *Biochemistry*, **38**, 11261–11270.
14. Takeda, S., Yamazaki, H., Seog, D. H., Kanai, Y., Terada, S. & Hirokawa, N. (2000). Kinesin superfamily protein 3 (KIF3) motor transports fodrin-associating vesicles important for neurite building. *J. Cell. Biol.* **148**, 1255–1265.
15. Wu, X. Q., Xu, L. & Hecht, N. B. (1998). Dimerization of the testis brain RNA-binding protein (translin) is mediated through its C terminus and is required for DNA- and RNA-binding. *Nucl. Acids Res.* **26**, 1675–1680.
16. VanLoock, M. S., Yu, X., Kasai, M. & Egelman, E. H. (2001). Electron microscopic studies of the translin octameric ring. *J. Struct. Biol.* **135**, 58–66.
17. Lee, S. P., Fuior, E., Lewis, M. S. & Han, M. K. (2001). Analytical ultracentrifugation studies of translin:

analysis of protein–DNA interactions using a single-stranded fluorogenic oligonucleotide. *Biochemistry*, **40**, 14081–14088.

18. Pascal, J. M., Chennathukuzhi, V. M., Hecht, N. B. & Robertus, J. D. (2001). Mouse testis-brain RNA-binding protein (TB-RBP): expression, purification, and crystal X-ray diffraction. *Acta Crystallog. sect. D*, **57**, 1692–1694.

19. Otwinowski, Z. & Minor, W. (1997). Processing of X-ray diffraction data collected in oscillation mode. *Methods Enzymol.* **276**, 307–326.

20. Terwilliger, T. C. & Berendzen, J. (1999). Automated M.A.D. and MIR stucture solution. *Acta Crystallog. sect. D*, **55**, 849–861.

21. Collaborative Computational Project, Number 4 (1994). The CCP4 suite: programs for protein crystallography. *Acta Crystallog. sect. D*, **50**, 760–763.

22. Kleywegt, G. J. & Jones, T. A. (1994). Halloween—masks and bones. In *Proceedings of the CCP4 study weekend: from first map to final model* (Bailey, S., Hubbard, R. & Waller, D., eds), pp. 59–66, Science and Engineering Research Council, Daresbury Laboratory, Warrington, UK.

23. Jones, T. A., Zou, J.-Y., Cowan, S. W. & Kjeldgaard, M. (1991). Improved methods for building protein models in electron density maps and the location of errors in these models. *Acta Crystallog. sect. A*, **47**, 110–119.

24. Brunger, A. T., Adams, P. D., Clore, G. M., DeLano, W. L., Gros, P., Grosse-Kunstleve, R. W. *et al.* (1998). Crystallography and NMR system: a new software suite for macromolecular structure determination. *Acta Crystallog. sect. D*, **54**, 905–921.

25. Laskowski, R. A., McArthur, M. W., Moss, D. S. & Thornton, J. M. (1993). PROCHECK: a program to check the stereochemical quality of protein structures. *J. Appl. Crystallog.* **26**, 283–291.

26. Colovos, C. & Yeates, T. O. (1993). Verification of protein structures: patterns of nonbonded atomic interactions. *Protein Sci.* **2**, 1511–1519.

27. Kraulis, P. J. (1991). MOLSCRIPT: a program to produce both detailed and schematic plots of protein structure. *J. Appl. Crytallog.* **2**, 946–950.

28. Esnouf, R. M. (1999). Further additions to MolScript version 1.4, including reading and contouring of electron-density maps. *Acta Crystallog. sect. D*, **55**, 938–940.

29. Merrit, E. A. & Bacon, D. J. (1997). Raster3D: photo-realistic molecular graphics. *Methods Enzymol.* **277**, 505–524.

30. Barton, G. J. (1993). ALSCRIPT: a tool to format multiple sequence alignments. *Protein Eng.* **6**, 37–40.

Edited by R. Huber